



## **Non-uniform modal decomposition of thin-walled members by the constrained finite element method**

Sandor Adány<sup>1</sup>

### **Abstract**

In this paper a new method, the constrained finite element method is applied for the modal decomposition of thin-walled members. With the help of this method the thin-walled member can be enforced to deform in accordance with some predefined criteria. In stability analysis, thus, it becomes straightforward to directly study various buckling types, for example flexural buckling, flexural-torsional buckling, distortional buckling, etc., as desired by the user. The main focus of the paper is on the special feature of the method that modal decomposition can be performed for non-uniform members, too, more specifically, for any members built of from prismatic segments. The connecting segments can have different cross-sections. Moreover, the segments can be constrained into different deformation modes, that is the enforced deformations may vary from segment to segment. In the paper the constrained finite element method is briefly presented first, then numerical examples are shown where either the cross-section and/or the constraining is changing along the member length.

### **1. Introduction**

The complex behavior of thin-walled members can beneficially be characterized as the interaction of various simpler phenomena. This is the reason why the deformations of a thin-walled beam or column member are frequently categorized into simpler, yet practically meaningful deformation classes: global (G), distortional (D), local-plate (L), shear (S) and transverse extension (T) modes, based on some characteristic features of the deformations. In many practical cases it is the G, D and L modes there are most important, other modes, even though if they are characterized by smaller displacements, sometimes have crucial importance, e.g., in the torsional behavior of hollow sections.

In case of thin-walled members, due to their high slenderness, instability phenomena have pronounced importance. In many cases the buckling takes place in a complex form, and the decomposition of the complex buckling shape into simpler classes has been found to be useful for capacity prediction and appears either implicitly or explicitly in current thin-walled design standards, too. For critical load calculation of thin-walled beams or columns the constrained finite strip method (cFSM) was proposed as a tool, see Ádány and Schafer (2008) or Ádány and

---

<sup>1</sup> Associate Professor, Budapest University of Technology and Economics, <sadany@epito.bme.hu>

Schafer (2014a,b). It is based on the semi-analytical finite strip method (Cheung 1976, Hancock 1978), but mechanically defined constraints are applied which can enforce the member to deform in accordance with a desired deformation, e.g. to buckle in flexural, lateral-torsional, or distortional mode. Another popular method that is able to perform modal decomposition is the generalized beam theory (GBT), see e.g. Silvestre et al. (2011). Though these methods are useful tools, they have limitations. One such limitation is that they cannot properly handle cross-section changes. Though there have been various attempts to extend GBT or FSM for members with holes, which can be considered as a special type of cross-section change, e.g. Eccher et al. (2009), Casafont et al. (2011), Cai and Moen (2015), Casafont et al. (2015), it is fair to say that FSM and GBT are developed principally for prismatic members.

Lately a novel decomposition method, the constrained finite element method (cFEM) has been proposed, see Ádány (2016a,b,c,d), Ádány et al (2016), Visy and Ádány (2017), Ádány (2017), Ádány et al (2017). The new method uses the idea of cFSM, however, the constraining procedure is applied for shell finite elements. Since shell finite element method can handle almost any practical problem in the realm of thin-walled members, the proposed cFEM can provide a solid platform to handle previously unresolved problems, such as the modal decomposition of members with cross-section changes, which is in the main focus of the actual paper.

In this paper first the cFEM is briefly summarized, then its application for members with varying cross-section is demonstrated by numerical examples. The examples prove the simple applicability of cFEM for piece-wise prismatic members, as well as show the potential benefits of applying non-uniform constraining along the members length can also be seen.

## 2. cFEM essentials

### 2.1 Shell finite element for cFEM

The constrained finite element method (cFEM) is essentially a shell finite element method, in which modal decomposition can be performed similarly as in cFSM. First, therefore, finite element discretization is necessary, as illustrated in Fig 1.

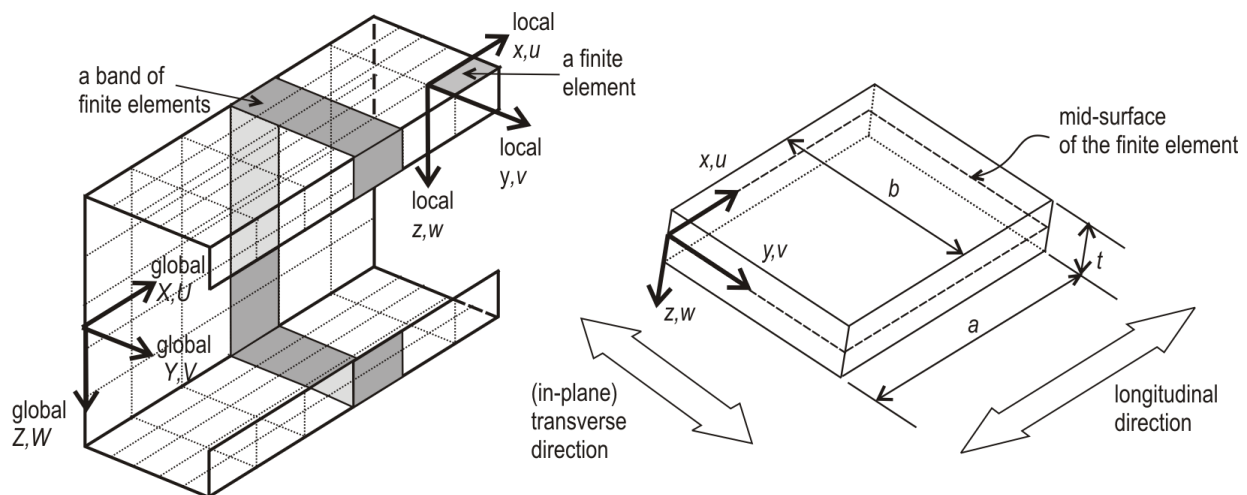


Figure 1: FEM discretization and basic notation

Since the constraining procedure that leads to modal decomposition is intended to perform as in cFSM, a special shell finite element is necessary. Though unusual in shell finite elements, the element of cFEM distinguishes the two perpendicular directions, as illustrated in Fig 1. The two in-plane (i.e.,  $u$  and  $v$ ) and one out-of-plane (i.e.  $w$ ) displacement functions are expressed as a product of transverse and longitudinal base functions, as follows.

$$u(x, y) = u_{11}N_{y,1}^{(1)}N_{x,1}^{(2)} + u_{13}N_{y,2}^{(1)}N_{x,1}^{(2)} + u_{21}N_{y,1}^{(1)}N_{x,2}^{(2)} + \quad (1)$$

$$+ u_{23}N_{y,2}^{(1)}N_{x,2}^{(2)} + u_{31}N_{y,1}^{(1)}N_{x,3}^{(2)} + u_{33}N_{y,2}^{(1)}N_{x,3}^{(2)}$$

$$v(x, y) = v_{11}N_{y,1}^{(1)}N_{x,1}^{(3)} + v_{13}N_{y,2}^{(1)}N_{x,1}^{(3)} + v_{31}N_{y,1}^{(1)}N_{x,3}^{(3)} + v_{33}N_{y,2}^{(1)}N_{x,3}^{(3)} + \quad (2)$$

$$+ \vartheta_{z11}N_{y,1}^{(1)}N_{x,2}^{(3)} + \vartheta_{z13}N_{y,2}^{(1)}N_{x,2}^{(3)} + \vartheta_{z31}N_{y,1}^{(1)}N_{x,4}^{(3)} + \vartheta_{z33}N_{y,2}^{(1)}N_{x,4}^{(3)}$$

$$w(x, y) = w_{11}N_{y,1}^{(3)}N_{x,1}^{(3)} + w_{13}N_{y,3}^{(3)}N_{x,1}^{(3)} + w_{31}N_{y,1}^{(3)}N_{x,3}^{(3)} + w_{33}N_{y,3}^{(3)}N_{x,3}^{(3)} + \quad (3)$$

$$+ \vartheta_{x11}N_{y,2}^{(3)}N_{x,1}^{(3)} + \vartheta_{x13}N_{y,4}^{(3)}N_{x,1}^{(3)} + \vartheta_{x31}N_{y,2}^{(3)}N_{x,3}^{(3)} + \vartheta_{x33}N_{y,4}^{(3)}N_{x,3}^{(3)} -$$

$$- \vartheta_{y11}N_{y,1}^{(3)}N_{x,2}^{(3)} - \vartheta_{y13}N_{y,3}^{(3)}N_{x,2}^{(3)} - \vartheta_{y31}N_{y,1}^{(3)}N_{x,4}^{(3)} - \vartheta_{y33}N_{y,3}^{(3)}N_{x,4}^{(3)} -$$

$$- \vartheta_{xy11}N_{y,2}^{(3)}N_{x,2}^{(3)} - \vartheta_{xy13}N_{y,4}^{(3)}N_{x,2}^{(3)} - \vartheta_{xy31}N_{y,2}^{(3)}N_{x,4}^{(3)} - \vartheta_{xy33}N_{y,4}^{(3)}N_{x,4}^{(3)}$$

The elementary base functions are given as:

$$N_{x,1}^{(2)} = 1 - \frac{3x}{a} + \frac{2x^2}{a^2} \quad N_{x,2}^{(2)} = \frac{4x}{a} - \frac{4x^2}{a^2} \quad N_{x,3}^{(2)} = -\frac{x}{a} + \frac{2x^2}{a^2} \quad (4)$$

$$N_{x,1}^{(3)} = 1 - \frac{3x^2}{a^2} + \frac{2x^3}{a^3} \quad N_{x,2}^{(3)} = x - \frac{2x^2}{a} + \frac{x^3}{a^2} \quad N_{x,3}^{(3)} = \frac{3x^2}{a^2} - \frac{2x^3}{a^3} \quad N_{x,4}^{(3)} = -\frac{x^2}{a} + \frac{x^3}{a^2} \quad (5)$$

$$N_{y,1}^{(1)} = 1 - \frac{y}{b} \quad N_{y,2}^{(1)} = \frac{y}{b} \quad (6)$$

$$N_{y,1}^{(3)} = 1 - \frac{3y^2}{b^2} + \frac{2y^3}{b^3} \quad N_{y,2}^{(3)} = y - \frac{2y^2}{b} + \frac{y^3}{b^2} \quad N_{y,3}^{(3)} = \frac{3y^2}{b^2} - \frac{2y^3}{b^3} \quad N_{y,4}^{(3)} = -\frac{y^2}{b} + \frac{y^3}{b^2} \quad (7)$$

Therefore, the proposed element has 30 DOF: 6 for  $u$ , 8 for  $v$ , and 16 for  $w$ . Each corner node has 7 DOF (1 for  $u$ , 2 for  $v$ , and 4 for  $w$ ), while there are two additional nodes at  $(x,y)=(a/2,0)$  and  $(x,y)=(a/2,b)$  with one DOF per node for the  $u$  displacement. The DOF are illustrated in Fig 2.

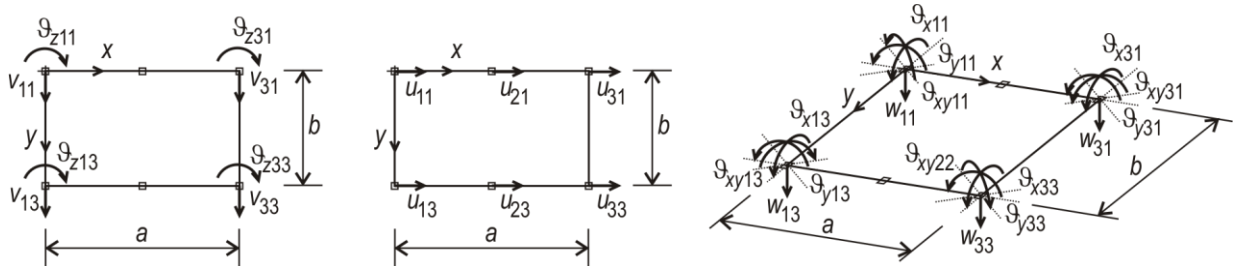


Figure 2: Nodal DOF of the proposed shell finite element

## 2.2 Constraining a shell element

The constraints that are embedded in cFSM are discussed in detail in Ádány and Schafer (2014a,b). It can be observed that the constraints are formulated by setting various displacement derivatives to zero. It can also be observed that the criteria are practically independent of the longitudinal shape functions, therefore, the same criteria can be used for cFEM, too. It is also important that the introduction of the mechanical criteria must lead to simple relationships in between the nodal displacement DOF, since this is a necessary condition if the mechanical criteria are intended to be exactly satisfied. The derivation of these relationships are given in Ádány (2016a), while here illustrated by a sample. As an example, in case of the no-longitudinal-extension criterion, the criterion is

$$\varepsilon_x = \frac{\partial u}{\partial x} = 0 \quad (8)$$

Using the assumed shape functions, the criterion can be written as:

$$\frac{dN_{x,1}^{(2)}}{dx}(u_{11}N_{y,1}^{(1)} + u_{13}N_{y,2}^{(1)}) + \frac{dN_{x,2}^{(2)}}{dx}(u_{21}N_{y,1}^{(1)} + u_{23}N_{y,2}^{(1)}) + \frac{dN_{x,3}^{(2)}}{dx}(u_{31}N_{y,1}^{(1)} + u_{33}N_{y,2}^{(1)}) = 0 \quad (9)$$

Considering Eqs (4)-(7), it is easy to conclude that the actual strain function is linear both in  $x$  and  $y$ . Therefore, the above expression can be written in the form:

$$C_{11}xy + C_{10}x + C_{01}y + C_{00} = 0 \quad (10)$$

with the  $C$  coefficients as follows:

$$\begin{aligned} C_{11} &= -4(u_{11} - u_{13} - 2u_{21} + 2u_{23} + u_{31} - u_{33})/b/a^2 \\ C_{10} &= 4(u_{11} - 2u_{21} + u_{31})/a^2 \\ C_{01} &= (3u_{11} - 3u_{13} - 4u_{21} + 4u_{23} + u_{31} - u_{33})/b/a \\ C_{00} &= -(3u_{11} - 4u_{21} + u_{31})/a \end{aligned} \quad (11)$$

The longitudinal strain is zero for any  $x$ - $y$  if (and only if) all the  $C$  coefficients are zero. This is satisfied only if

$$u_{11} = u_{21} = u_{31} \quad \text{and} \quad u_{13} = u_{23} = u_{33} \quad (12)$$

Thus, the no-longitudinal-strain criterion is expressed by the simple relationship in between the nodal degrees of freedom of the proposed shell element. All the other criteria can similarly be handled, see Ádány (2016a).

## 2.3 Constraining a band

In cFSM, if the constraints are applied, specific deformation modes are achieved. These special modes are essentially independent of the member length, which, in other words, means that the deformation modes can be characterized by the deformations of the cross-sections. That is why these special deformation modes are frequently referred as to *cross-section modes*. Since the constraining of cFSM and cFEM are essentially identical, the same cross-section modes can be achieved in cFEM as in cFSM.

The constraint matrices for a single shell element can be formed on the basis of the relationships between the various nodal degrees of freedom (as illustrated above). Once the elementary constraint matrices are defined, they can be assembled into a global constraint matrix for multiple elements. One way to do this is first to compile constraint matrix for one band of finite elements (where ‘band’ is given by Fig. 1), which leads to mode-specific deformation spaces for one band. Since these spaces are multi-dimensional, the base functions can be defined in multiple (in fact, infinite) ways. A practically useful and easy-to-understand way of defining the base function system for a specific deformation mode for one band is to take the cross-section modes (identical to the cross-section modes of cFSM), and then to add longitudinal displacement distribution with having unit ‘displacements’ and unit ‘displacement-derivatives’ at the end sections of the band.

As an example, if the mechanical constraints of the global bending mode (as formulated in Ádány and Schafer, 2014a,b) are applied for a band of finite elements, it leads to an 8-dimensional deformation space. Obviously, this space can be subdivided into a 4-dimensional minor-axis bending space, and a 4-dimensional major-axis bending space. In case of the minor-axis space the cross-section mode is characterized by rigid-body translation (along the major axis) and/or rigid-body rotation of the cross-section (around the minor axis). Thus, a possible way to create the base system is to set unit translation or rotation at one end of the band, while keeping zero translation and rotation elsewhere. The so-constructed base system for the minor-axis global bending space is demonstrated in Fig 3, by using the coordinate system and global displacements as shown in Fig 1. The base system for the major-axis global bending space can be constructed in the same way, illustrated in Fig 4. (It is important to underline here that in Figs 3-6 one *single band* of finite elements is shown, the length of which is  $a$ . The grid is used solely to make clearer how the deformed shape looks like.)

It is to observe that rigid-body rotation of a cross-section is associated with a linear warping distribution over the cross-section, therefore ‘rotation’ can also be interpreted as a specific ‘warping distribution’. This approach can readily be applied to construct base system for global torsion (see Fig 5) or distortional mode space (see Fig 6), where the characteristic transverse cross-section displacements and characteristic warping distributions are set to ‘unit’ and ‘zero’ values at the end sections.

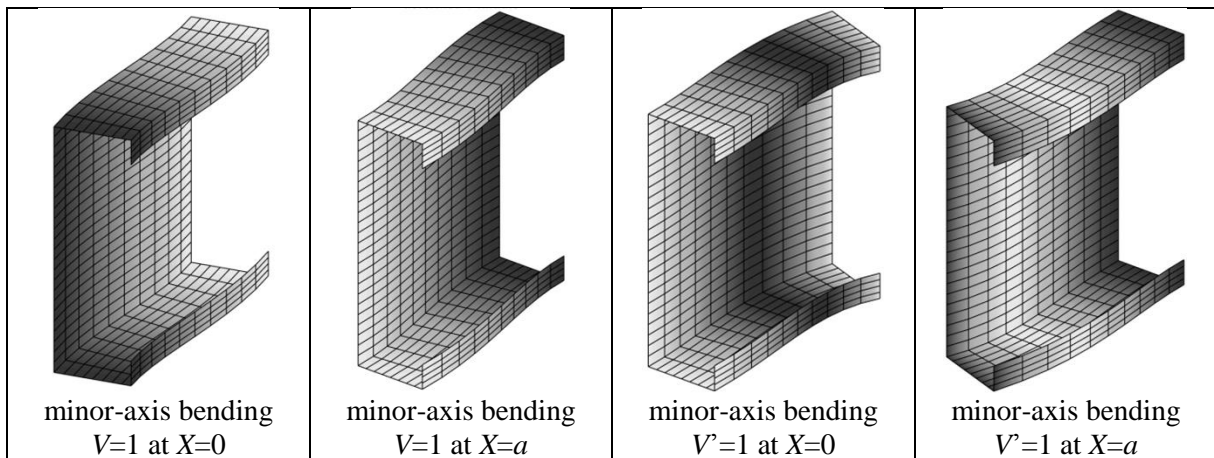


Figure 3: Base system for global minor-axis bending space of a band

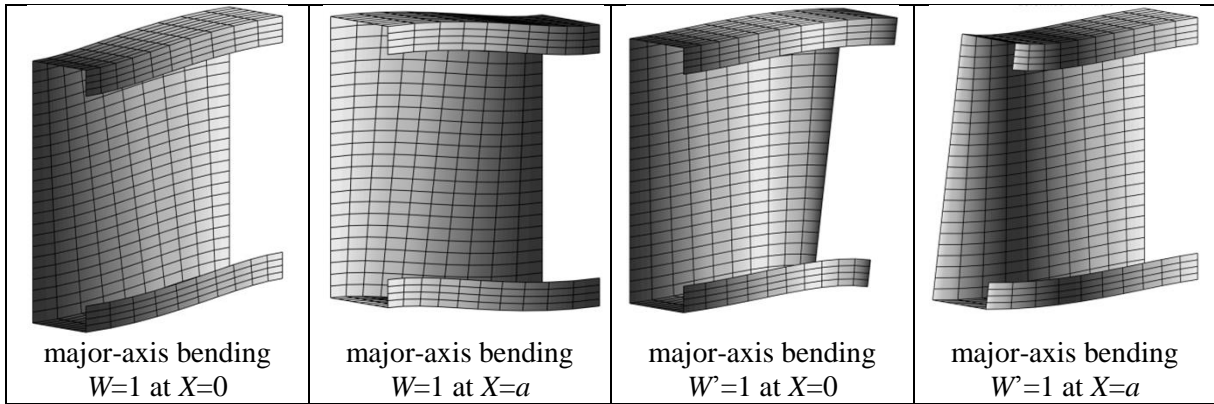


Figure 4: Base system for global major-axis bending space of a band

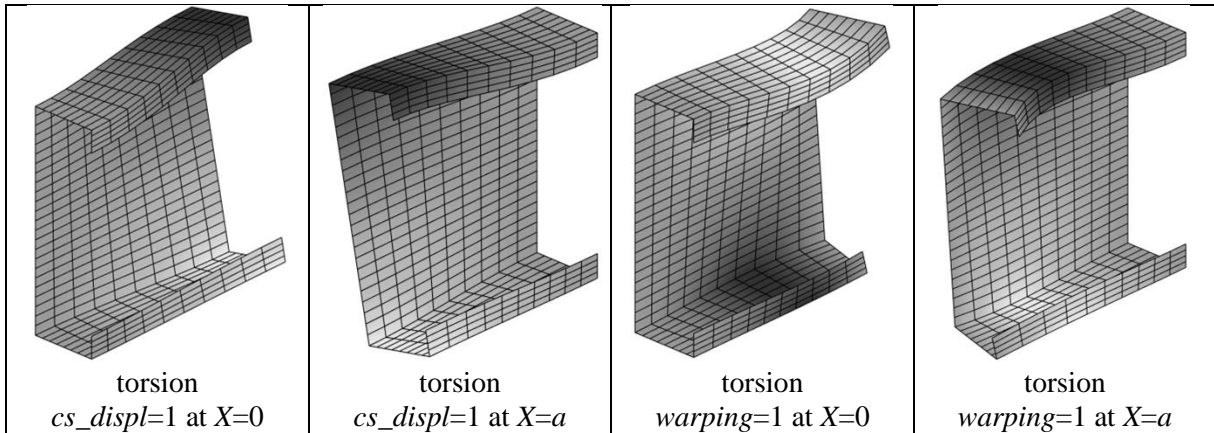


Figure 5: Base system for global torsion space of a band

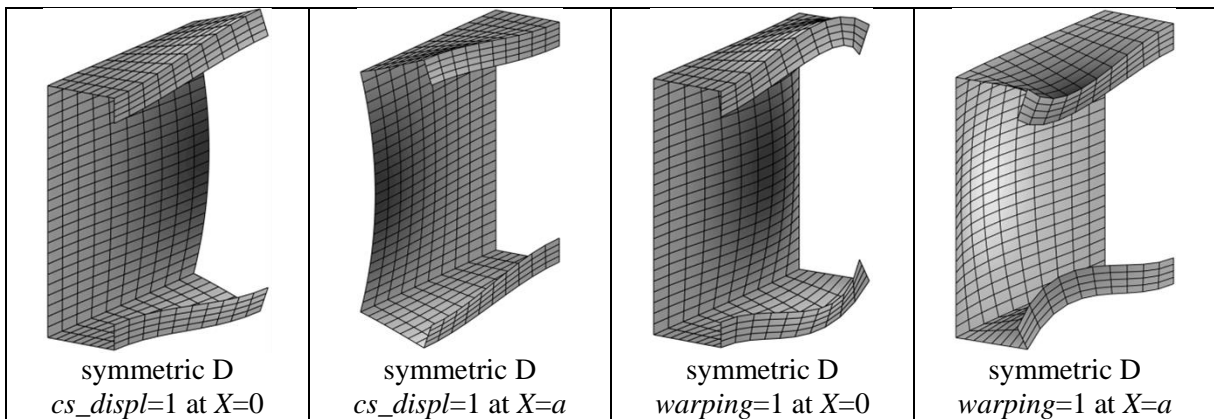


Figure 6: Symmetric distortional modes of a band of C section

## 2.4 Constraining a member

Since the member discretization is necessarily highly regular, and since constraining is performed from band by band, there is no any difficulty to place bands one after the other to form the member. In doing so, there is no any restriction with regard to cross-section shape or constraining, that is bands with different cross-sections and/or bands with different constraints can readily be connected. The only requirement is that the member should reasonably be modelled by rectangular shell finite elements.

## 2.5 Constrained buckling analysis

If FEM is applied to solve linear buckling problems (to get critical loads and buckling shapes), we need to construct first the local elastic and geometric stiffness matrices, by considering the 2D generalized Hooke's law (for the elastic stiffness matrix) and by considering the second-order strain terms (for the geometric stiffness matrix). The stiffness matrices can be determined analytically. The derivation of the element stiffness matrices is discussed in Visy and Ádány (2016). From the local stiffness matrices the member's (global) stiffness matrices (elastic and geometric,  $\mathbf{K}_e$  and  $\mathbf{K}_g$ ) can be compiled, by transformation to global coordinates and assembly.

Once the global stiffness matrices are established, linear buckling problem needs the solution of the following generalized eigen-value problem:

$$\mathbf{K}_e \Phi - \Lambda \mathbf{K}_g \Phi = \mathbf{0} \quad (13)$$

with

$$\Lambda = \text{diag} \langle \lambda_1 \lambda_2 \lambda_3 \dots \lambda_{nDOF} \rangle \quad \text{and} \quad \Phi = [\phi_1 \phi_2 \phi_3 \dots \phi_{nDOF}] \quad (14)$$

where  $\lambda_i$  is the critical load multiplier and  $\phi_i$  is the associated buckling shape, and  $nDOF$  denotes the number of degrees of freedom.

If model decomposition is to be performed, first the base system must be defined, as illustrated previously. The base system is to be summarized in the  $\mathbf{R}$  constraint matrix, the column vectors of the matrix being the modal base vectors of those sub-fields that are intended to be considered. With the help of the constraint matrix the FEM displacement field  $\mathbf{d}$  (including the eigen-buckling mode  $\Phi$ ) may be constrained to any modal  $\mathbf{d}_M$  deformation space via

$$\mathbf{d} = \mathbf{R}_M \mathbf{d}_M \quad (15)$$

where  $\mathbf{R}_M$  is a constraint matrix, which is the matrix representation of the constraining criteria, and 'M' might be G, D, L, S or T, or, in fact, 'M' might mean any combination of base vectors from any spaces. When constrained buckling analysis is performed, Eq (15) should be substituted into Eq (14), which leads to

$$\mathbf{R}_M^T \mathbf{K}_e \mathbf{R}_M \Phi_M - \Lambda \mathbf{R}_M^T \mathbf{K}_g \mathbf{R}_M \Phi_M = \mathbf{0} \quad (16)$$

which is another generalized eigen-value problem, given in the reduced M modal deformation space.

### 3. Demonstrative examples

#### 3.1 Example 1

Example 1 is about the buckling of a simple compressed member. The member has a square hollow cross-section, and is assumed to be connected by welded gusset plates and bolts at both member ends. The cross-section dimension is 100×100 mm (mid-line dimensions), the plate thickness is 2 mm, the length is 1300 mm. The gusset plate is 140 mm wide and 10 mm thick, centrally positioned w.r.t. the SHS section, and goes 200 mm beyond the end of the SHS member. The material of both the SHS member and the gusset plates is regular steel, with  $E=210\,000$  MPa,  $\nu=0.3$  and  $G=80\,769$  MPa.

Two bolts are assumed at both gusset plates, centrally positioned, 60 and 140 mm distance from the end of the SHS member. The bolts provide restraints. It is assumed that the gusset plates are fully restrained against lateral movement (i.e. perpendicularly to the plane of the plate) at the bolt positions, while elastically restrained in the plane of the plate. The elastic restraint is considered by a linear spring with assuming various stiffness values from 10 kN/mm to  $10^5$  kN/mm. It is also assumed that the bolts do not provide rotational restraint for the gusset plate.

The member is loaded by a concentric compression force of 1 kN. The force is transmitted by the bolts, assumed to be equally distributed between the two bolts.

First the buckling behavior of the SHS member is analyzed. The member is considered to be restrained by the end joints, including the gusset plates and the bolts (represented by springs). From modal decomposition point of view, therefore, the deformations of the SHS member are constrained into various spaces, while the gusset plates are unconstrained. In this way the supports conditions of the SHS member are realistically modelled, still, the modal decomposition capability of cFEM can lead to pure global, pure distortional or pure local buckling modes and critical forces. Some results are shown in Fig 7 (note, in all the cases first modes). For the given member configuration it is obviously the local plate buckling which is governing. Distortional buckling is possible, but at a high critical force level (which is typical in case of rectangular hollow sections). The global buckling is practically flexural buckling due to the high torsional rigidity of hollow sections. Obviously, the global critical force is highly dependent on the member length; in the actual case the member is relatively short, therefore the critical values are relatively high. Depending on the end joints, the lowest critical force might belong to in-plane (i.e., in the plane of the gusset plate) or to out-of-plane flexural buckling. If the bolts are assumed to provide highly rigid restraints against the in-plane translation of the gusset plate, the in-plane global critical force value is fairly high, however, as soon as smaller rigidity is assumed to be provided by the bolts, the in-plane flexural buckling force becomes smaller (while the other pure critical forces are practically unaffected by these springs).

In the actual example it is not only the SHS member, but also the gusset plate can buckle. If the deformations of the SHS member are totally filtered out (e.g., by allowing only rigid-body displacements of the SHS member), while the deformations of the gusset plates are allowed constrained or unconstrained, then the buckling behavior of the gusset plates can directly be analyzed. Fig 8 shows two cases: local-plate buckling is shown on the left, while pure flexural buckling on the right (note, in both cases first modes are shown). For the actual configuration the

flexural-type buckling might take place only at a rather high force level, but the plate-like buckling is associated with a critical force level comparable to that of the SHS member itself.

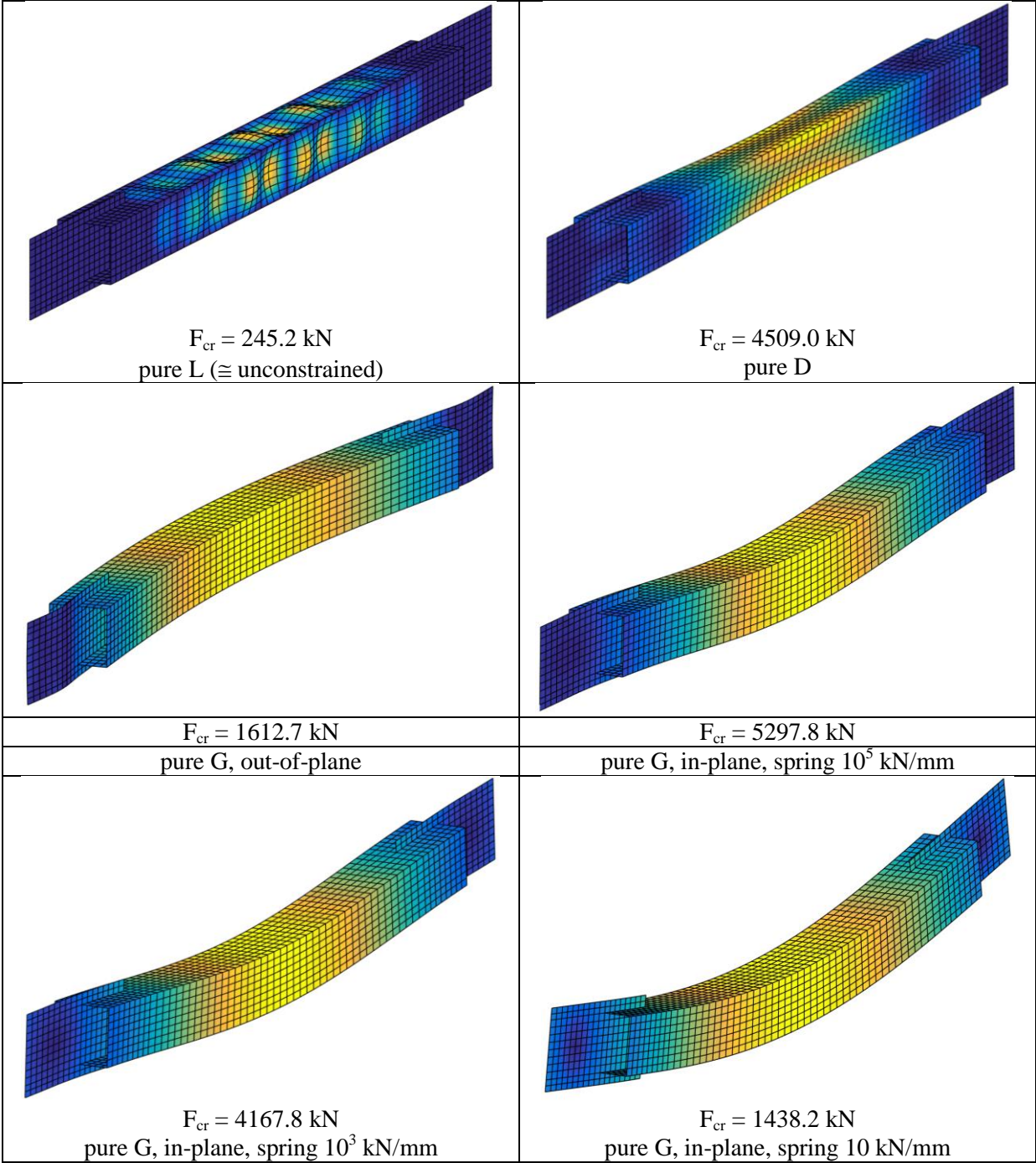


Figure 7: Example 1, pure G, D and L buckling of the SHS member

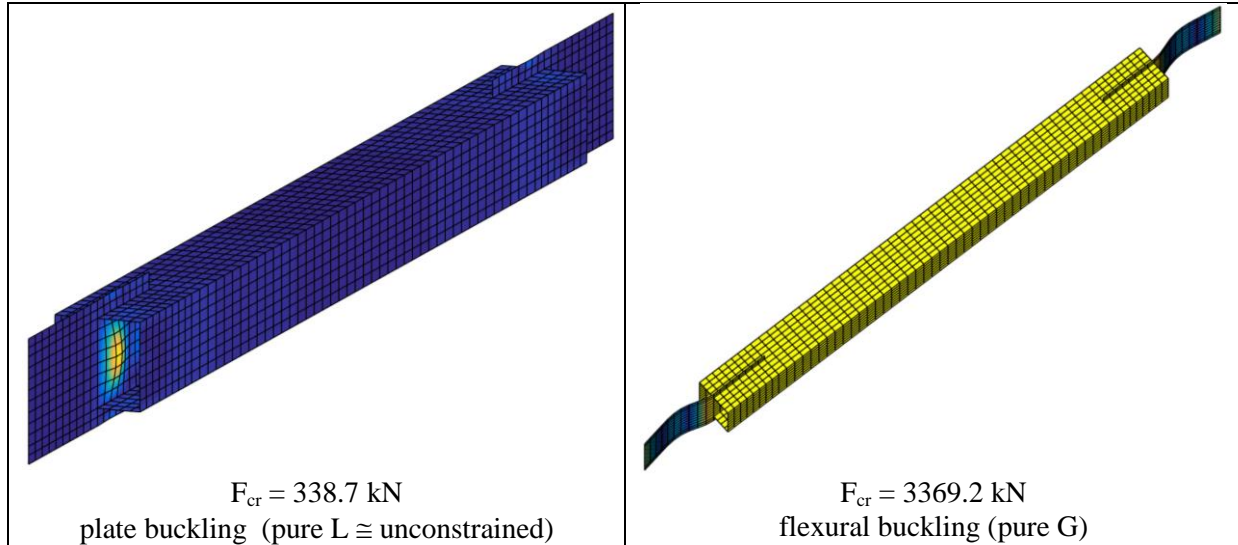


Figure 8: Example 1, buckling of the gusset plate

### 3.2 Example 2

Example 2 is discussing the buckling behavior of a lipped channel member, which is strengthened by plates connecting the two flange lips at discrete intervals. A possible model of the strengthened segment is a rectangular hollow section, thus, the member to be analyzed here consisted of lipped channel and RHS segments placed one after the other.

The dimensions of the considered lipped channel sections are as follows: web depth is 150 mm, flange width is 100 mm, lip length is 15 mm, thickness is 2 mm, and member length is 1200 mm. The material is regular steel, with  $E=210\,000$  MPa,  $\nu=0.3$  and  $G=80\,769$  MPa.

Strengthening plates are applied, the thickness of which is equal to that of the lipped channel (i.e., 2 mm), while the width is 40 mm. The material is regular steel. The number of strengthening plates varies, but the plates are always evenly distributed along the member length. The member is supported in a globally and locally hinged way at its end cross-sections. Concentric compression forces are applied at the member ends, uniformly distributed over the end cross-sections.

Critical loads are calculated by applying various constraints to the member. Table 1 summarizes the calculated critical loads, while Figs 9-11 show some buckled shapes.

If the deformations are constrained into the L space, see first row of Fig 9 and the last column of Table 1, the strengthening plates have negligible effect on the behavior, which is dominated by the buckling of the web due to the longitudinal compressive stresses.

In Fig 9 minor-axis flexural buckling samples are also shown, calculated by constraining the whole member into G space, or, more specifically, to those sub-space of G space which is defined by the minor-axis bending modes. Though the presence of strengthening plates slightly increases the critical load value, the behavior is hardly affected. The increased critical load value is due to the slightly increased bending stiffness and the slightly modified stress distribution. As

the numbers of Table 1 show, the maximum critical force increase is approx. 10 % for this actual example, even if a fairly large number of strengthening plates is considered.

Table 1: Example 2, critical loads

strengthening plate number	minor-axis buckl critical load N/mm <sup>2</sup>	flexural-tors buckl critical load N/mm <sup>2</sup>	distortional buckl critical load N/mm <sup>2</sup>	plate buckling critical load N/mm <sup>2</sup>
0	2142.8	760.4	194.5	175.0
1	2204.7	809.1	314.2	175.0
2	2235.6	1767.1	635.2	175.0
3	2267.7	2967.6	1161.3	175.0
4	2301.0	4154.7	1920.1	175.0
5	2335.3	5046.2	2955.8	175.0

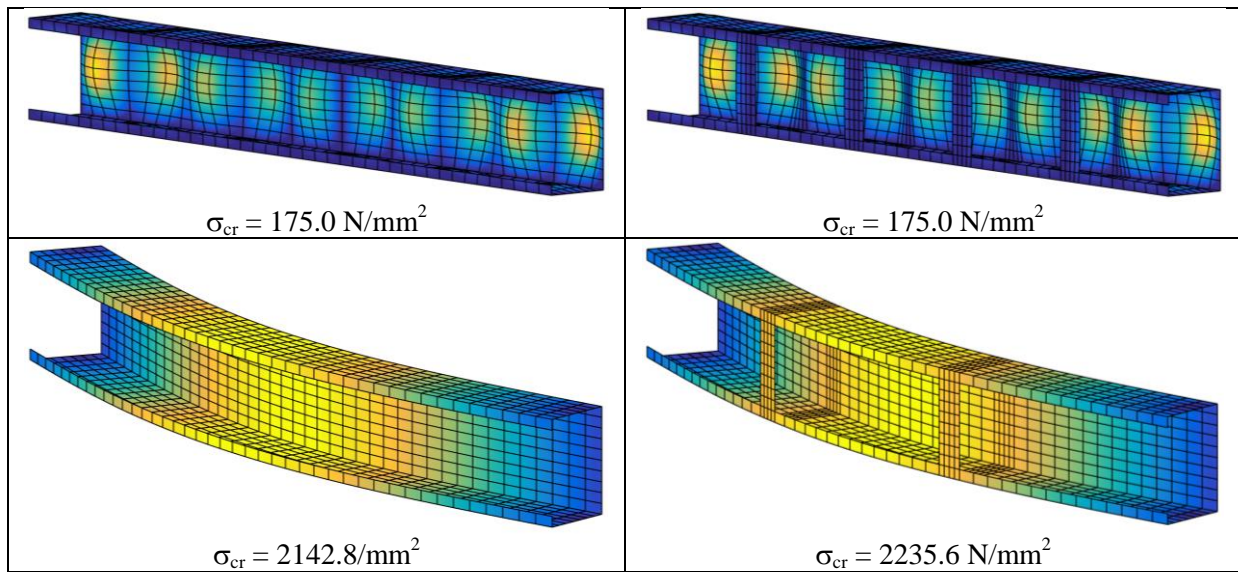


Figure 9: Example 2, minor axis flexural buckling and local plate buckling samples

Unlike minor-axis flexural buckling or local plate buckling, the distortional buckling and flexural-torsional buckling are significantly influenced by the strengthening plates. Fig 10 shows distortional buckling shape samples for various number of strengthening plates, when the whole member is constrained into D space. Even though both C and RHS sections have distortional modes, they are not compatible, i.e., when a C and RHS segment is connected longitudinally, it is not possible to have distortional behavior for both the C and RHS member. Considering that the pure distortional critical force of a C section is much lower than that of a RHS of otherwise similar dimensions, what happens in this actual example is, hence, that the RHS segments remain practically rigid, while the C segments show the classic distortional deformations, see Fig 10. From the viewpoint of the lipped channel member, therefore, the application of a strengthening plate is more-or-less equivalent with the application of a clamped support. The strengthening plates reduce the characteristic length of the buckling waves: the more strengthening plates are applied, the smaller the buckling wave length is. Accordingly, the distortional critical values go up drastically with the introduction of strengthening plates.

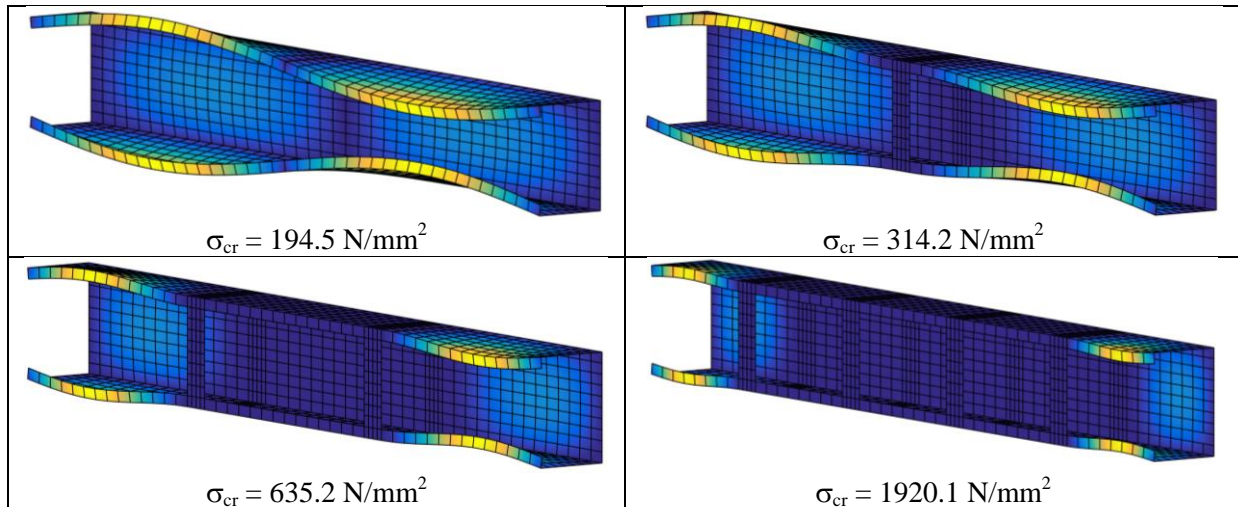


Figure 10: Example 2, distortional buckling samples

In case of flexural-torsional behavior, the constraining is not evident. Flexural-torsional behavior requires (in this example) major-axis flexure and torsion about the longitudinal axis of the member. Both these modes are typically categorized as global, more precisely, shear-free global, when the cross-sections remain rigid and there is no in-plane (membrane) shear in any plates of the member. While major-axis flexure exists for both C and RHS, torsion mode exists only for C, since torsion of a closed cross-section requires shear deformations. There is one exception, however, when the whole member (or segment) is rotated as a rigid body. When the whole member has a closed cross-section, the rigid-body displacement of the member must be prevented by the supports, but if the member is consisted of segments with different cross-sections, then a segment might displace as a rigid body. In this example, therefore, the member is constrained as follows: C-shaped segments are constrained into global major-axis bending and global torsion space, while closed segments are constrained into global major-axis bending and rigid-body torsion space.

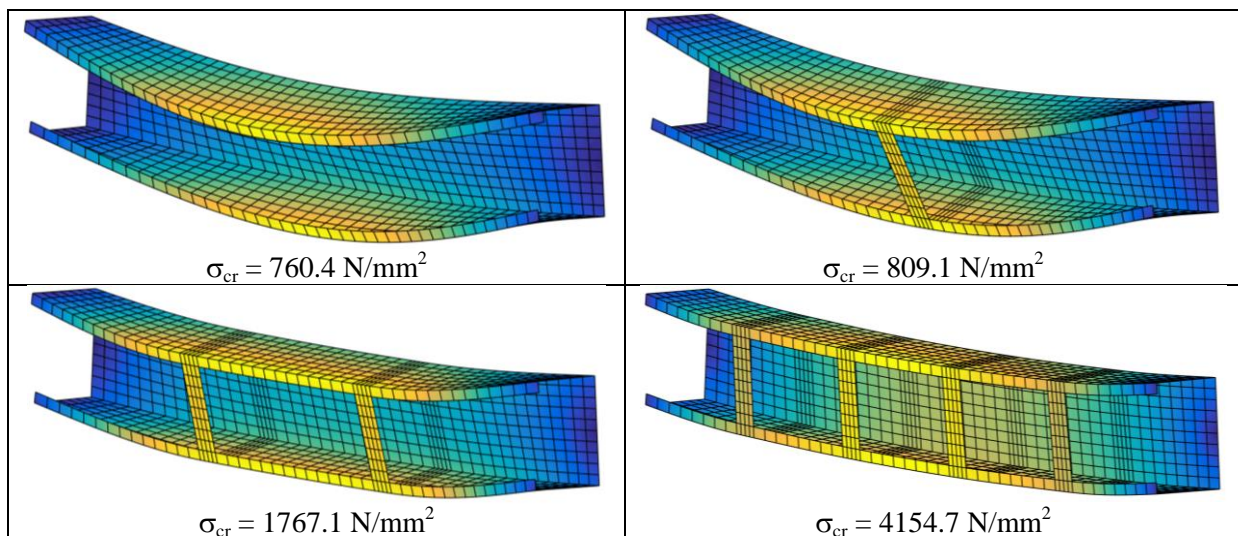


Figure 11: Example 2, flexural-torsional buckling samples

The resulting critical values are summarized in Table 1, while buckled shapes are shown in Fig 11. The general tendency is that: the larger the number of strengthening plates, the larger the critical load value is. The increase of critical load value is rather significant.

### 3.3 Example 3

Example 3 is essentially identical to Example 2. The only difference is that shear deformations are allowed. In-plane (membrane) shear deformations are considered for two reasons: (1) in-plane shear deformations do exist, hence, it is more realistic to consider them, (2) in the actual example it might be too optimistic to assume that the strengthening plates are connected to the lips in a perfectly rigid way (e.g., if the connection is made by screws, some flexibility of the connection cannot be avoided).

Since the effect of strengthening plates is almost negligible in case of minor-axis flexural buckling and local plate buckling, only distortional and flexural-torsional behavior will be discussed here. In order to study the importance of the shear rigidity of the strengthening plates, 3 material models are considered for the strengthening plates: (1) isotropic material, (2) orthotropic material with shear modulus  $1/10^{\text{th}}$  of that of the isotropic material, and (3) (2) orthotropic material with shear modulus  $1/1000^{\text{th}}$  of that of the isotropic material (i.e., material with an almost negligible shear rigidity).

In case of distortional buckling, the deformations are constrained into the union of D and S spaces, considering primary and secondary S spaces, too. Note, primary S space is built up from shear bending spaces, shear torsion space, and shear distortion space, see Ádány (2013), Ádány and Schafer (2014a,b). The calculated critical loads (i.e., lowest values) are summarized in Table 2, where the corresponding values from Example 2 are also repeated to make the comparison easier. Some buckled shapes are presented in Fig 12 (first row). As both the numerical values and buckled shapes suggest, the closed segments do not mean any more a clamped support for the C segments, consequently, the member is more flexible and the critical values are considerably smaller w.r.t. the ones in Example 2. The reduction of the critical load (compared to those of Example 2) is dependent on the parameters, but for the actual example it is in between 5% and 30% for the cases with strengthening plate(s). Though the consideration of shear deformations, especially together with reduced shear rigidity, has considerable effect on the behavior and on the critical load values, still, the strengthening plates are very effective in increasing the distortional buckling load.

Table 2: Example 3, critical loads for distortional buckling

strengthening plate number	no shear	with shear	with shear	with shear
	N/mm <sup>2</sup>	$G=E/2/(1+\nu)$ N/mm <sup>2</sup>	$G=E/2/(1+\nu)/10$ N/mm <sup>2</sup>	$G=E/2/(1+\nu)/1000$ N/mm <sup>2</sup>
0	194.5	192.9	192.9	192.9
1	314.2	297.6	286.6	279.4
2	635.2	572.3	546.6	528.6
3	1161.3	986.3	934.2	901.3
4	1920.1	1529.9	1436.8	1381.3
5	2955.8	2201.3	2062.9	1987.4

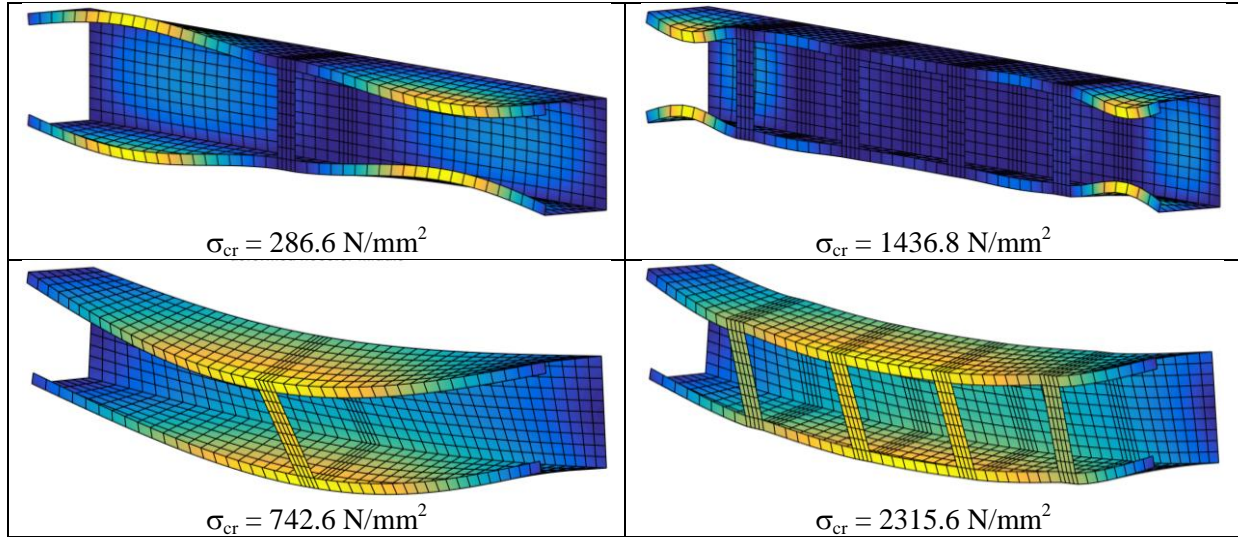


Figure 12: Example 3, buckling with shear samples,  $G=E/2/(1+\nu)/10$

Table 3 summarizes the critical load values for flexural-torsional buckling, while some buckled shapes are shown in Fig 12. It is evident that the consideration of shear deformations makes the member considerably more flexible. The reduction of the flexural-torsional critical load (compared to those of Example 2) is dependent on the parameters, but for the actual example it is in between 8% and 46% for the cases with strengthening plate(s). Though the consideration of shear deformations, especially together with reduced shear rigidity, has considerable effect on the behavior and on the critical load values, still, the strengthening plates are very effective in increasing the flexural-torsional buckling load.

Table 3: Example 3, critical loads for FT buckling

strengthening plate number	no shear	with shear	with shear	with shear
	$N/mm^2$	$G=E/2/(1+\nu)$ $N/mm^2$	$G=E/2/(1+\nu)/10$ $N/mm^2$	$G=E/2/(1+\nu)/1000$ $N/mm^2$
0	760.4	737.4	737.4	737.4
1	809.1	743.7	742.6	742.3
2	1767.1	1284.7	1216.4	1192.9
3	2967.6	1918.3	1768.3	1715.9
4	4154.7	2544.1	2315.6	2234.2
5	5046.2	3117.1	2836.7	2735.4

#### 4. Summary

In this paper the constrained finite element method has been applied to solve buckling problems of members with non-uniform cross-sections. Through the numerical examples the modal decomposition capability of the method has been demonstrated for piece-wise prismatic thin-walled members. cFEM makes it possible to build a single realistic shell model (e.g., including realistic support conditions), while still to utilize modal decomposition. The results also show the potential benefit of applying varying constraints along the member length: this allows calculating

the critical load value directly to a certain type of buckling in a certain part of the member. Thus, unlike in a regular shell finite element buckling analysis, it is not necessary to check hundreds of mostly interacted buckling modes to find a desired mode, but this desired mode can be found in way which is more direct, more objective, and more efficient.

## Acknowledgments

The work was conducted with the financial support of the OTKA K108912 project of the Hungarian Scientific Research Fund.

## References

- Ádány S. (2012). Global Buckling of Thin-Walled Columns: Analytical Solutions based on Shell Model, *Thin-Walled Structures*, Vol 55, pp 64-75.
- Ádány, S., Schafer, B.W. (2006a). Buckling mode decomposition of single-branched open cross-section members via Finite Strip Method: derivation, *Thin-Walled Structures* **44**(5), pp. 563-584.
- Ádány, S., Schafer, B.W. (2006b). Buckling mode decomposition of single-branched open cross-section members via Finite Strip Method: application and examples, *Thin-Walled Structures*, **44**(5), pp. 585-600.
- Ádány, S., Schafer, B.W. (2008). A full modal decomposition of thin-walled, single-branched open cross-section members via the constrained finite strip method, *Journal of Constructional Steel Research*, 64 (1), pp. 12-29..
- Ádány S. (2013). Decomposition of in-plane shear in thin-walled members, *Thin-Walled Structures* (2013), Vol 73, pp 27-38.
- Ádány S., Schafer B.W. (2014a). Generalized constrained finite strip method for thin-walled members with arbitrary cross-section: Primary modes, *Thin-Walled Structures*, Vol 84, pp. 150-169.
- Ádány S., Schafer B.W. (2014b). Generalized constrained finite strip method for thin-walled members with arbitrary cross-section: Secondary modes, orthogonality, examples, *Thin-Walled Structures*, Vol 84, pp. 123-133.
- Ádány S. (2014). Constrained finite element method: demonstrative examples on the global modes of thin-walled members, *Proceedings of the Twenty-Second International Speciality Conference on Cold-Formed Steel Structures*, (eds. R. A LaBoube, W.W. Yu) St. Louis, Missouri, USA, Nov 5-6, 2014. pp. 67-81.
- Ádány S. (2016a). Shell element for constrained finite element analysis of thin-walled structural members, *Thin-Walled Structures*, Volume 105, August 2016, Pages 135-146.
- Ádány S. (2016b). Constrained finite element method for the modal analysis of thin-walled members with holes, *Proceedings of the Annual Stability Conference, SSRC, Orlando, Florida, April 12-15, 2016.* paper no: 40. p. 20.
- Ádány S. (2016c). Understanding the buckling behavior of thin-walled members by using the constrained finite element method, *Proceedings of the 7th International Conference on Coupled Instabilities in Metal Structures* (Ed. B. W. Schafer), Baltimore, Maryland, November 7-8, 2016.
- Ádány S. (2016d). Constrained finite element method for the analysis of shear buckling of thin-walled members, *Proceedings of the Eighth International Conference on Steel and Aluminium Structures* (Ed. B. Young), Hong Kong, China, December 7–9, 2016.
- Ádány S., Visy D., Nagy R. (2016). Buckling solutions for thin-walled members by using the constrained finite element method: demonstrative examples, *Proceedings of the International Colloquium on Stability and Ductility of Steel Structures, SDSS 2016*, (eds. D. Dubina, V. Ungureanu), Timisoara, Romania, May 30 – June 1, 2016, pp. 51-58.
- Visy D., Ádány S. (2017). Local elastic and geometric stiffness matrices for the shell element applied in cFEM, submitted to *Periodica Polytechnica ser. Civil Engineering*
- Ádány S. (2017). Constrained shell Finite Element Method for thin-walled members, Part1: constraints for a single band of finite elements, submitted to *Thin-Walled Structures*
- Ádány S. Visy D., Nagy R. (2017). Constrained shell Finite Element Method: application to linear buckling analysis of thin-walled members, submitted to *Thin-Walled Structures*
- Cai J., Moen C.D. (2015). Generalized beam theory buckling analysis for members with holes, Eighth International Conference on Advances in Steel Structures, Lisbon, Portugal, July 22-24, 2015, paper no:86, p. 18.

- Casafont M., Marimon F., Pastor M.M., Ferrer M. (2011). Linear buckling analysis of thin-walled members combining the Generalised Beam Theory and the Finite Element Method, *Computers and Structures*, 89(21-22), Nov 2011, pp. 1982-2000.
- Casafont M., Bonada J., Pastor M.M. and Roure F. (2015). GBT calculation of distortional and global buckling of cold-formed steel channel columns with multiple perforations, *Proceedings of the Eighth International Conference on Advances in Steel Structures*, Lisbon, Portugal, July 22-24, 2015, paper no:87, p. 18.
- Cheung, Y.K. (1976). Finite strip method in structural analysis, Pergamon Press, 1976.
- Eccher, G., Rasmussen, K.J.R. Zandonini, R. (2009). Geometric nonlinear isoparametric spline finite strip analysis of perforated thin-walled structures, *Thin-Walled Structures*, Volume 47, Issue 2, February 2009, Pages 219-232.
- Hancock, G.J. (1978). Local, Distortional, and lateral buckling of I-beams, *ASCE Journal of structural engineering*, 104(11), pp. 1787-1798.
- Li, Z., Schafer B.W. (2009). Finite Strip Stability Solutions for General Boundary Conditions and the Extension of the Constrained Finite Strip Method, in *Trends in Civil and Structural Engineering Computing*. 2009. Stirlingshire, UK: Saxe-Coburg Publications.
- Li, Z., Schafer, B.W. (2010). Buckling analysis of cold-formed steel members with general boundary conditions using CUFSM: Conventional and constrained finite strip methods, *Proceedings of the 20th International Specialty Conference on Cold-Formed Steel Structures - Recent Research and Developments in Cold-Formed Steel Design and Construction*, p. 17.
- Silvestre N., Camotim D., Silva N.F. (2011). Generalized Beam Theory revisited: from the kinematical assumptions to the deformation mode determination, *Int. Journal of Structural Stability and Dynamics*, 11(5), Oct 2011, pp. 969-997.